XVIII[èmes] Journées Nationales Génie Côtier – Génie Civil
Anglet, 2024
DOI:10.5150/jngcgc.2024.045 *© Editions Paralia CFL*
disponible en ligne – http://www.paralia.fr – available online

Tidal and geological controls on longshore sediment transport along the north of the Médoc coast, SW France

Arthur ROBINET [1], Alexandre NICOLAE LERMA [1], Déborah IDIER [1], Ivana MINGO [2], Vincent MARIEU [2], Bruno CASTELLE [2]

1. Bureau de Recherches Géologiques et Minières, 24 Avenue Léonard de Vinci, 33600 PESSAC.
   a.robinet@brgm.fr
2. Université de Bordeaux, CNRS, UMR EPOC 5805, Allée Geoffroy Saint-Hilaire, CS 50023, 33615 Pessac, France.

Abstract:
The north of the Médoc coast, SW France, is a sandy coast with complex environment settings including an irregular bathymetry, shallow banks and rocky outcrops, and adjacent to a km-scale estuary. This coast is strongly affected by marine erosion and exhibits dramatic erosion trends, with shoreline retreats reaching locally several meters per year for decades. New coastal management scenarios for the next years, or even decades, need to be investigated. This will require the implementation and use of reduced-complexity shoreline change models. They are valuable tools to simulate past and future shoreline changes at time scales from seasons to centuries. These models usually rely on time and space integration of wave-driven longshore sediment transport, which is one of the main drivers of shoreline change along sandy coasts on the long-term. This longshore transport is computed from breaking wave conditions, which are controlled by several physical processes occurring within the nearshore area. However, the control of local environmental settings on breaking waves is usually over-simplified in reduced-complexity shoreline change models, if not neglected. This study investigates the sensitivity of the wave-driven longshore sediment transport along the north of the Médoc coast to different physical processes affecting the wave propagation. Results revealed that on a monthly scale the bathymetry and the bottom friction play a predominant role on longshore sediment transport patterns. In contrast, the contribution of tide-driven water levels is lower on this timescale, and even less for contribution of the tide-driven currents.

Keywords:
Wave model, SWAN, Longshore sediment transport, Bathymetry, Bottom friction, Tide, Water level, Currents, Sandy coast, Estuary, Gironde, Médoc.

1. Introduction

The north of the Médoc coast, SW France, is a high-energy macrotidal open sandy coast located just south the km-scale Gironde estuary. This sandy coast is significantly threatened by marine erosion and exhibits dramatic erosion trends, with shoreline retreats reaching locally several meters per year for decades. For many years, some urbanized areas along this coast have been exposed to this erosion and local authorities have been undertaking various management strategies (sea wall, groin, nourishment) to mitigate the shoreline retreat. However, as erosion persists around these protected areas, the implementation of these strategies is becoming increasingly compromised (cost, technical feasibility). New coastal management scenarios for the next years, or even decades, need to be investigated. Reduced-complexity shoreline change models are often mentioned as valuable alternatives to complex physical-based morphodynamic models to simulate past and future shoreline changes at time scales from seasons to centuries and to address this need. By including simplified parameterizations of the main physical processes driving shoreline changes at the scales of interest, reduced-complexity models run with short computing times, suffer little from error accumulation through temporal and spatial scales, and include a small number of parameters to be calibrated. However, to ensure that the results are obtained within an acceptable range of errors, the knowledge of the minimal physical processes to be included in these models remains crucial, particularly when applied to complex environments. The north of the Médoc coast (SW France) is a particularly challenging area to setup a shoreline change model. The strong flood and ebb currents (about 0.5-1 m/s in the nearshore) due to the proximity of the estuary and the complex nearshore bathymetry (including shallow banks and rocky outcrops) significantly affect the offshore wave transformation up to breaking and induce a strong alongshore variability in the breaking wave conditions and longshore sediment transport (e.g. ROBINET *et al*., 2020). This work introduces sensitivity analyses aiming to assess the respective contribution of the tide (sea level fluctuations, currents) and the nearshore bathymetry (irregular iso-contours, shallow banks and outcrops) on the longshore sediment transport along this coast. To do this, a modelling framework relying on the spectral wave model SWAN (BOOIJ *et al*., 1999) and two nested computational grids is used to propagate the waves over the nearshore water domain of our study site. The longshore sediment transport is computed using the breaking waves conditions extracted along coast. Some physical processes included in a first reference SWAN simulation are alternatively switched off or altered in additional simulations and the resulting impacts on the longshore sediment transport are analyzed.

2. Study Site

The study site consists of almost 13-km of sandy coastline located along the southern side of end of the Gironde estuary, one of the largest European estuaries (Figure 1). The

bathymetry offshore this coastline is complex as evidenced by the irregular iso-contours shown in Figure 1. The bathymetry is characterised by the presence of a km-scale area of shallow depths (north part of the large computational grid) bordered with the two main channels of the Gironde estuary on the north and south. Although the south channel is far less pronounced than the north one, it still represents one of the major bathymetric irregularities found directly offshore the studied coastline (northwest part of the small computational grid). Below bottom elevation of -15 m relative to the mean sea level (MSL) the iso-contours in the north part of the study site show a northwest-southeast orientation, which progressively shifts to the south to a north-south orientation. Finally, numerous shallow banks and rocky bottom areas can be found at various locations of the nearshore domain (Figure 1).

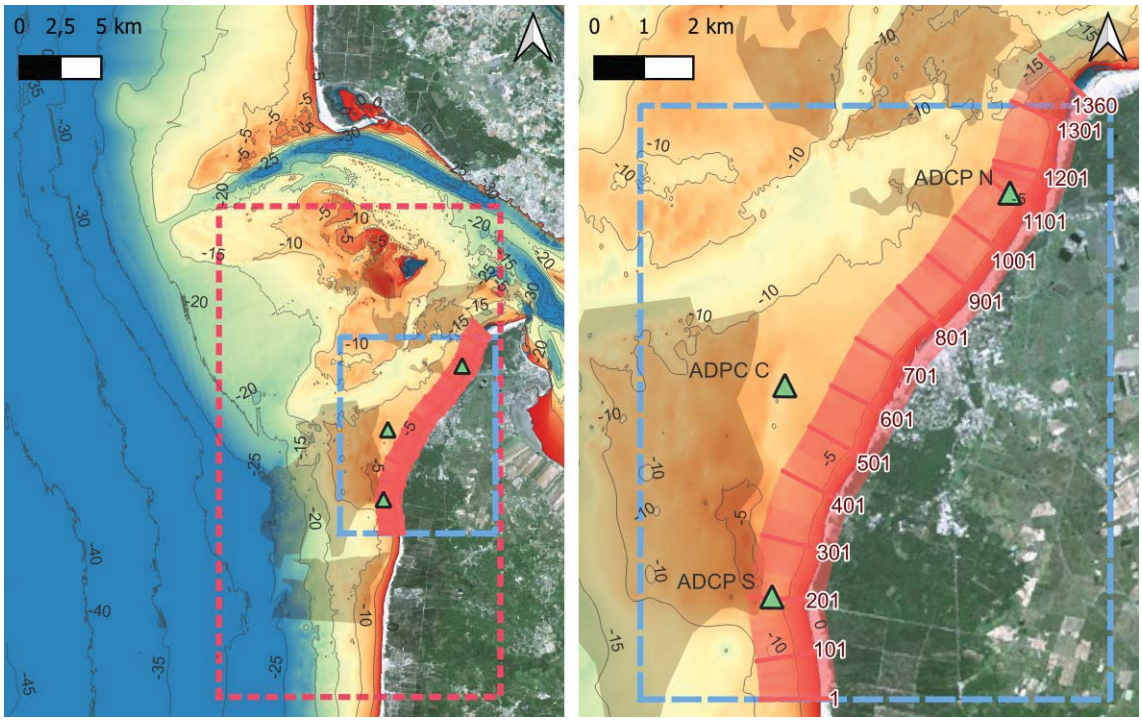

Figure 1. Maps of the study site showing the large (red extent) and small (blue extent) SWAN computational grids, the bathymetry relative to the mean sea level, the 5-m-spaced bathymetric iso-contours, the rocky bottom areas (grey patches), the transects (red lines) where longshore sediment transport is computed, and location of three ADCP (green triangles) used for wave comparisons.

The tidal is semi-diurnal and microtidal with a tidal range varying from 1.5 to 5.5 m during neap and spring tide, respectively (CASTAING & ALLEN, 1981). The tide drives strong currents with speeds potentially reaching 1 m/s (HOWA, 1987). These currents are maximized and reverse during ebb and flow. This coast is exposed to high-energy, seasonally modulated waves with larger and longer waves coming from the west sector in winter and smaller and shorter waves coming from the west-northwest

sector in summer. Deep water wave characteristics are quite similar to those of the Cap Ferret beach (located 90 km to the south), which shows winter significant wave height (H_s) and peak wave period (T_p) around 2.4 m and 12.8 s, and summer H_s and T_p around 1.11 m and 9 s, respectively (CASTELLE *et al.*, 2017).

3. Data

The bathymetry used to set the bottom level over the large and small SWAN computational grids is provided by SHOM using the approximatively 20-m resolution "*HOMONIM phase 3*" topo-bathymetric product (SHOM, 2022). The rocky bottom areas are provided by SHOM using the "*Natures de fond*" product (SHOM, 2023). In this study it was chosen to consider the bottom types named "*Roche*", "*Cailloutis*" and "*Graviers*" as rocky bottom (grey patches in Figure 1). The offshore wave conditions used to force the large SWAN computational grid along its open boundaries are provided by IFREMER through the MARC platform (https://marc.ifremer.fr) using the best estimate product of an hourly wave forecast relying on the spectral wave model WAVEWATCH III. The maps of tide-driven water level relative to the mean sea level and currents used to force the large and small SWAN computational grids are provided by IFREMER and are taken from the above-mentioned WW3 wave forecast best estimate product. Wave conditions measured by three ADCP (named North, Center and South; green triangles in Figure 1) during a 5-weeks field campaign from 24/08/2022 to 04/10/2022 are used to assess the ability of the reference SWAN simulation to reproduce the nearshore wave fields. Details regarding this field campaign and the processing of the collected data are provided in VANDENHOVE *et al.,* (2024).

4. Methods

4.1 Simulation set-up

A first SWAN simulation was set up to provide a reference simulation. In this simulation, the open boundaries of the large computational grids were forced every 500 m with wave conditions (H_s, T_p, D_p) spatially interpolated from the WW3 wave forecast. The bottom level over the computational grids was defined using the measured bathymetry from the SHOM. Wave energy dissipation by bottom friction was switched on in combination with the formulation of MADSEN et al. (1988). Distinct values of friction coefficient k_n were used for sandy bottom ($k_{n,s}$) and rocky bottom ($k_{n,r}$). As the literature regarding recommended values for k_n is rare, suitable values were here obtained by a light trial-and-error approach by comparing simulated and observed wave conditions at the three ADCP locations. Values of $k_{n,s} = 0.01$ for sandy bottom and $k_{n,r} = 0.2$ for rocky bottom provided a good match between simulated and observed wave conditions and were used hereafter. A time varying and uniform water level was used in SWAN for both computational grids. The water level at each simulation time step was

determined by averaging the water level of WW3 wave forecast grid points located inside the large computational grid extent. Time and spatial varying current fields were also used in SWAN. The current fields were extracted at each simulation time step from the WW3 wave forecast. Four additional simulations were set up identically to the reference simulation, but each time switching off or altering one of the physical processes mentioned above. The characteristics of these simulations relative to the reference simulation are provided in Table 1. In the simulation "*Idealized bathymetry*", the bathymetry was derived by propagating a Dean profile from the shoreline seaward. The Dean profile coefficients were optimized against an average beach profile computed from the SHOM bathymetry between the 0-m and 8-m iso-contours. In the simulation "*Uniform friction*" the rocky bottom friction coefficient was assumed equal to the one of the sandy bottom, i.e. $k_{n,s} = k_{n,r} = 0.01$. In the simulation "*Constant water level*", the water level was set equal to the mean sea level throughout the simulation.

Table 1. Characteristics of simulations used for sensitivity analysis, with boldface indicating the physics modified in relation to the reference simulation.

Simulation name	***Bathymetry***	***Bottom friction***	***Water level***	***Currents***
Reference	*Real*	*Variable*	*Variable*	*Variable*
Idealized bathymetry	***Idealized***	*Variable*	*Variable*	*Variable*
Uniform friction	*Real*	***Uniform***	*Variable*	*Variable*
Constant water level	*Real*	*Variable*	***Constant***	*Variable*
No current	*Real*	*Variable*	*Variable*	***Absence***

4.2 Longshore sediment transport computation

A set of 10-m alongshore-spaced cross-shore transects (Figure 1) was used to extract the wave conditions just before the breaking point, which was defined as the point where the ratio of Hs to the water depth (γ_b) is equal to 0.73. Then, the longshore sediment transport is computed at each transect using the CERC formula (USACE, 1984).

4.3 Simulation periods

The reference simulation was firstly run over the period of the ADCP deployment (24/08/2022 - 04/10/2022) to compare simulated and observed wave conditions, and to assess the model skill. Then, the reference simulation and the additional simulations were run over the period 01/11/2022 - 30/11/2022. This second period was chosen as it shows alternating periods of calm and highly energetic wave conditions, which was not the case for the period of the ADCP deployment.

5. Results

5.1 Model skill of the reference simulation

The Table 2 provides some statistics resulting from the comparison of wave conditions measured at the three ADCP locations with the wave conditions simulated with the reference simulation. Simulated H_s are in a good agreement with observations. However, as evidenced by Figure 2, at ADCP N and ADCP C the model seems to fail at reproducing the high-tide wave height during periods of large incoming waves (e.g. from 06/09/2022 to 13/09/2022). Based on Table 2, the skill of the model in reproducing T_p seems poor. However, a visual comparison of the time series of T_p (not shown) reveals that the observed T_p is quite noisy, especially at ADPC S. It also shows that, on the contrary, simulated and observed T_p time series match well apart from the few noisy periods. Finally, the skill of the model in reproducing D_m is apparently low with important positive and negative bias at ADPC C and ADCP S, respectively. This means that the simulated waves at ADPC C and ADCP S comes too often from the northwest direction and from the northwest direction, respectively. Apart from the rough tuning of the sand and rocky bottom friction coefficients, no other calibration was performed. Thus, there is space for improvement of the model skill through a more-in-depth and intensive calibration. However, this was out of the scope of this study that focuses more on the relative impact on longshore transport of changing slightly the physics included in the simulations rather than investigating the absolute values of longshore transport of the reference simulation.

Table 2. Statistics resulting from comparisons of wave conditions observed at the three ADPC and simulated with the reference simulation.

Wave statistic	***ADCP***	***RMSE***	***MAE***	***Bias***	***R^2***
H_s	*N*	*0,33*	*0,21*	*-0,15*	*0,86*
	C	*0,25*	*0,19*	*-0,11*	*0,85*
	S	*0,15*	*0,12*	*0,04*	*0,84*
T_p	*N*	*1,89*	*1,20*	*0,28*	*0,62*
	C	*2,33*	*1,30*	*0,37*	*0,52*
	S	*3,31*	*1,96*	*1,33*	*0,33*
D_m	*N*	*13,42*	*10,50*	*-2,93*	*0,04*
	C	*19,89*	*17,47*	*17,30*	*0,10*
	S	*17,72*	*13,53*	*-11,66*	*0,10*

5.2 Sensitivity analyses on longshore sediment transport

The timestacks of longshore sediment transport obtained for each simulation over the period 01/11/2022 - 30/11/2022 are shown in Figure 3. In these representations, the sub-daily oscillations visible along the temporal direction correspond to a modulation by the

tide level and/or the currents. In contrast the short-spatial-scale oscillations visible along the spatial direction (i.e. the transect number) is likely less physical-based and related to small mismatches between the transect orientation (roughly perpendicular to the coastline) and the normal to the average orientation of the bathymetric iso-contours in shallow depths, which is felt by approaching waves before breaking. For this reason, this spatial variability occurring at the scale of few tens of transects, i.e. few hundreds of meters, is disregarded in the following analyses.

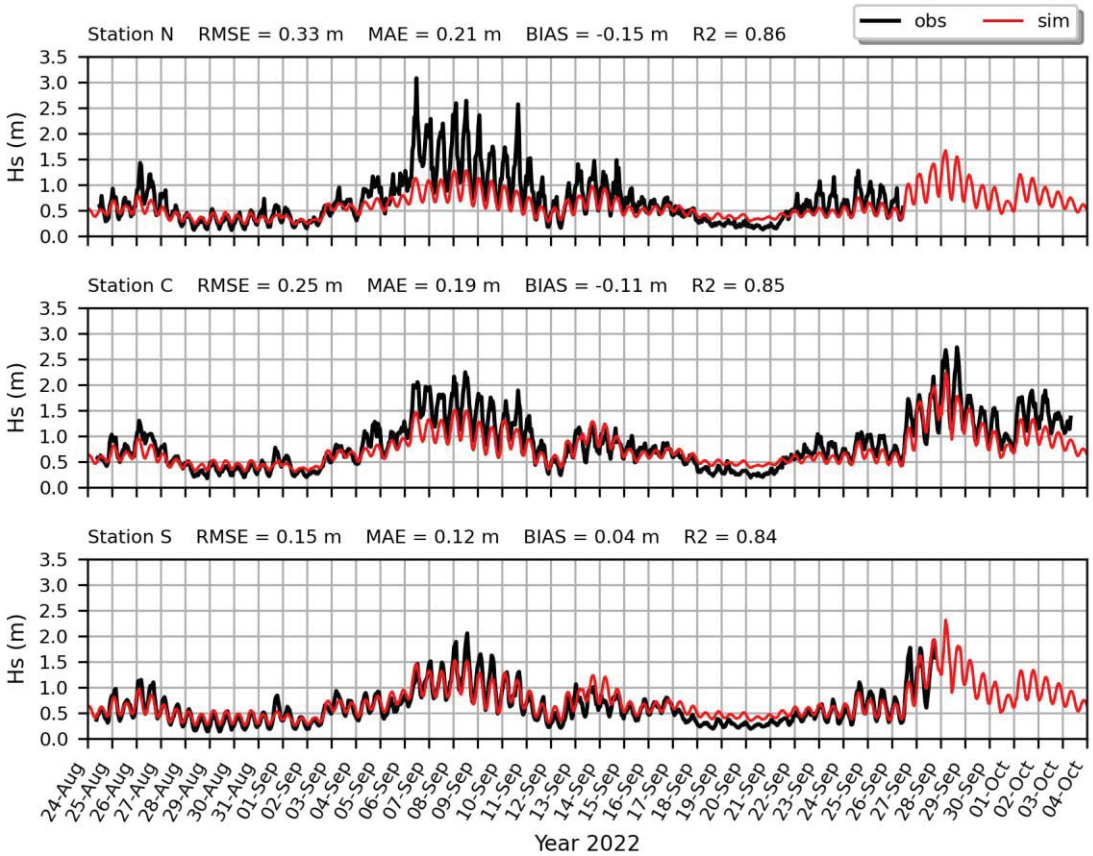

Figure 2. Comparison of time series of H_s observed at the three ADCP (black) and simulated with the reference simulation (red).

Overall, all the timestacks share some common patterns of longshore transport (Figure 3). Indeed, in all simulations we observe the occurrence of the six sequences of some days during which the longshore transport magnitude is maximized (approximatively centered on the 4, 7, 17, 22, 24 and 28/11/2022). We also observe that the longshore transport is essentially directed northward except in the very south part of the domain, south of transect no. 200, where the longshore transport is directed southward over a longshore extent of several tens of transects. For the simulation “Idealized bathymetry” this shift in terms of longshore transport direction occurs a bit more north. This behavior is also depicted in Figure 4, which shows the time-averaged longshore transport per

transect over the study period. Indeed, for the later simulation there is a large shift in terms of monthly-averaged longshore transport direction that occurs approximatively between transects no. 220 and no. 275, while for the other simulations it occurs approximatively between transects no. 40 and no. 120. This suggests that the large shallow bank visible offshore transects no. 200 and 400 (Figure 1), which is not present in the idealized bathymetry, strongly controls the local longshore transport direction and, by deduction, the breaking wave direction.

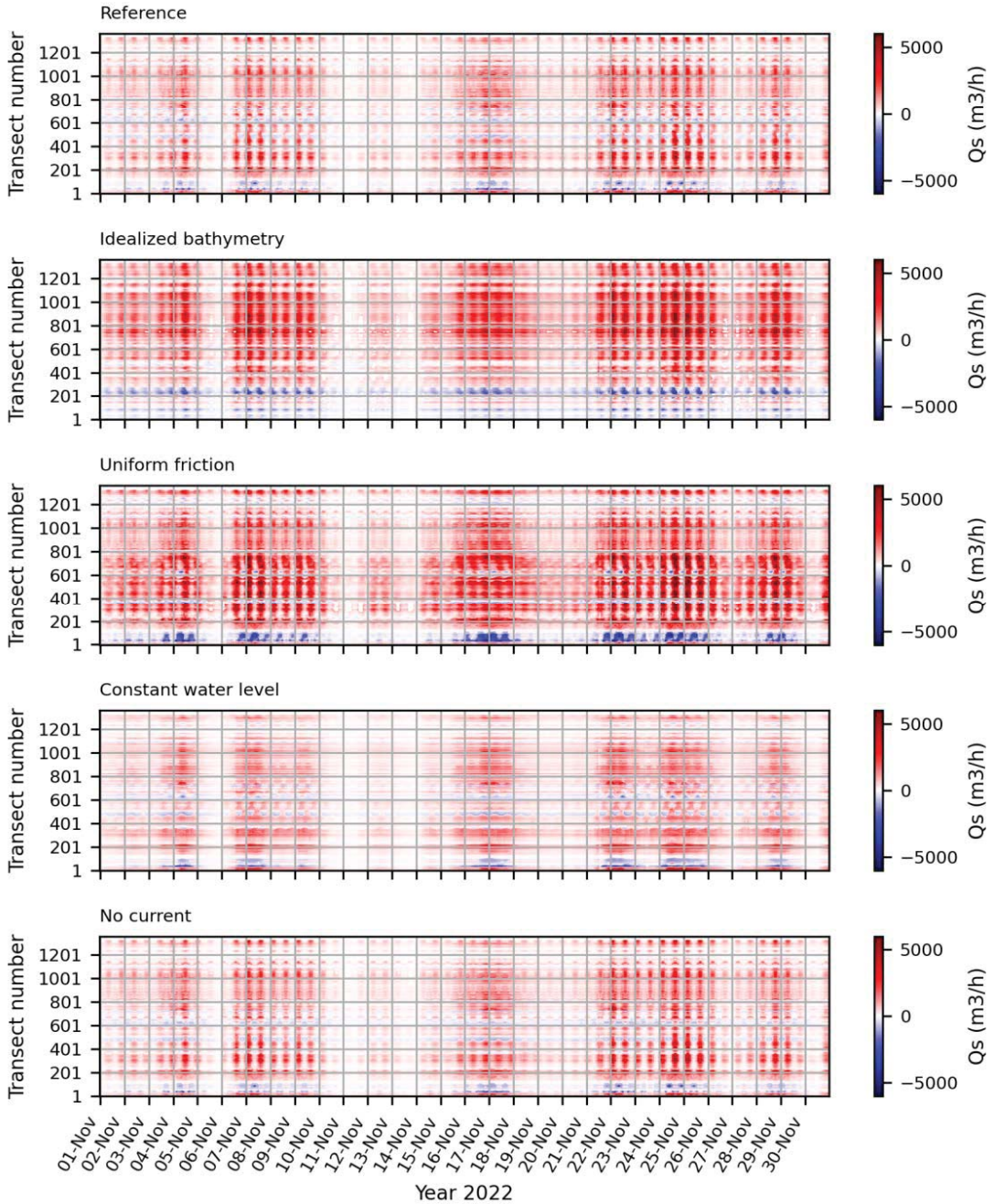

Figure 3. Timestacks of longshore sediment transport for different simulation set-ups. Positive (negative) value denotes a northward (southward) longshore transport.

A more detailed analysis of the timestacks (Figure 3) and of the spatial variability of the monthly-averaged longshore transport (Figure 4) reveals that the simulations "Idealized bathymetry" and "Uniform friction" contrast with the reference simulation by an overall increase in longshore transport magnitude. This increase mainly occurs north of transect no. 501 for simulation "Idealized bathymetry" and south of transect no. 801 for simulation "Uniform friction". This suggests that simplifying the bathymetry by smoothing out bathymetric irregularities (e.g. shallow sandbanks, rocky outcrops, channels) and/or neglecting the increase in friction over rocky bottoms can significantly boost the magnitude of longshore transport as this study site.

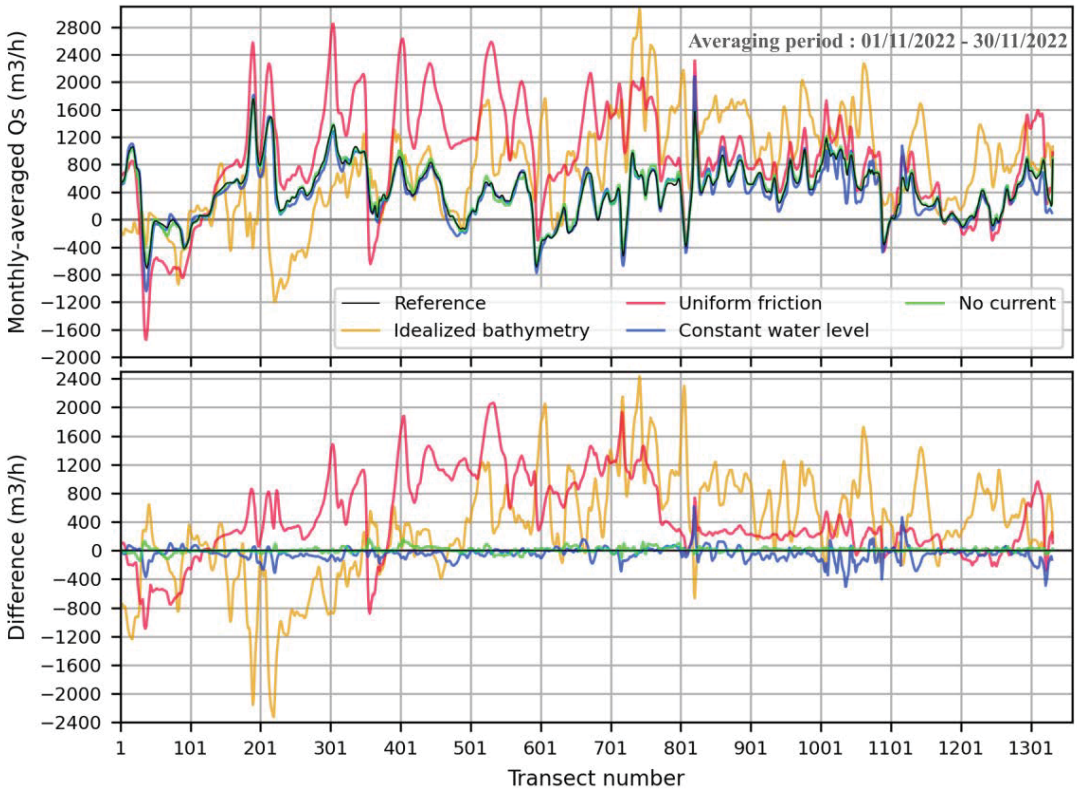

Figure 4. Time-averaged of the longshore sediment transport at each transect over the study period (top) and difference with respect to the reference simulation (bottom).

The simulations "Constant water level" and "No current" lead to patterns of longshore transport more similar to those of the reference simulation (Figure 3, Figure 4). Figure 3 reveals also that enforcing a constant water level in the simulation remove most of the sub-daily oscillations observed in the reference simulation except between transects no. 401 and 801. This suggests that in this area the tide controls the longshore transport on a sub-daily scale not only though the modulation of the water level but also though the modulation of the currents. Elsewhere, the tide might control the longshore transport on a sub-daily scale mainly though the modulation of the water level. Finally, on a monthly

scale, the average longshore transport seems to be only slightly sensitive to the inclusion of the tidal water level variation, and even less to the inclusion of tidal currents (Figure 4). This is because these processes induce almost symmetrical changes on wave-driven longshore sediment transport at the scale of a tide cycle (not shown).

6. Conclusion

This study showed that on a monthly scale the bathymetry and the bottom friction play a predominant role on longshore sediment transport patterns along the north of the Médoc coast. In contrast, the contribution of tide-driven water levels is lower on this timescale, and even less for contribution of the tide-driven currents. Repeating this work with longer simulation periods may confirm that these findings can be extrapolated to longer timescales, which is likely the case. Our results should help future implementation of shoreline change models at this coast, indicating which physical processes are to be included by order of priority and according the degree of approximation desired.

7. References

BOOIJ N., RIS R. C., HOLTHUIJSEN L. H. (1999). *A third-generation wave model for coastal regions: 1. Model description and validation.* Journal of geophysical research: Oceans, 1999, vol. 104, no C4, 7649-7666. doi.org/10.1029/98JC02622

CASTAING P., ALLEN G.P. (1981). *Mechanisms controlling seaward escape of suspended sediment from the Gironde: A macrotidal estuary in France.* Marine Geology 40, 101–118. doi:10.1016/0025-3227(81)90045-1

CASTELLE B., BUJAN S., FERREIRA S., DODET G. (2017). *Foredune morphological changes and beach recovery from the extreme 2013/2014 winter at a high-energy sandy coast*. Marine Geology, vol. 385, 41-55. doi:10.1016/j.margeo.2016.12.006

HOWA H. (1987). *Le littoral du Nord Medoc, (Gironde) - Evolution d'une cote sableuse en érosion.* Thesis University or Bordeaux I, Soc. Geol. France, 258.

ROBINET A., CASTELLE B., IDIER D., HARLEY M.D., SPLINTER K.D. (2020). *Controls of local geology and cross-shore/longshore processes on embayed beach shoreline variability.* Marine Geology 422, 101–118. doi.org/10.1016/j.margeo.2020.106118

SHOM (2022). *MNT topo-bathymétrique côtier de l'estuaire de la Gironde – Aval (Projet HOMONIM).* https://dx.doi.org/10.17183/MNT_COTIER_GIRONDE_AVAL_HOMONIM_20m_WGS84

SHOM (2023). *Natures de fond au 1/50 000*.

https://diffusion.shom.fr/donnees/sedimentologie/natures-de-fond.html

VANDENHOVE M., CASTELLE B., NICOLAE LERMA A., MARIEU V., MINGO I., ROBINET A., MARTINS K., BUJAN S., MAZEIRAUD V. (2024). *Caractérisation de l'hydrodynamisme des plages et des petits fonds du littoral au sud de l'estuaire de la Gironde à partir de mesures in situ*. XVIII^{èmes} Journées Nationales Génie Côtier – Génie Civil, Anglet, (*article soumis*).